CHEMISTRY OF MATERIALS

Article

pubs.acs.org/cm

Synthesis of SnS Thin Films by Atomic Layer Deposition at Low Temperatures

In-Hwan Baek,[†,‡] Jung Joon Pyeon,[†,§] Young Geun Song,[†,⊥] Taek-Mo Chung,[∥] Hae-Ryoung Kim,[#] Seung-Hyub Baek,[†,¶] Jin-Sang Kim,[†] Chong-Yun Kang,[†,§] Ji-Won Choi,[†] Cheol Seong Hwang,[‡] Jeong Hwan Han,[∥,⊗] and Seong Keun Kim*[,†]

[†]Center for Electronic Materials, Korea Institute of Science and Technology, Seoul 02792, South Korea

[‡]Department of Materials Science and Engineering, and Inter-University Semiconductor Research Center, Seoul National University, Seoul 08826, South Korea

[§]KU-KIST Graduate School of Converging Science and Technology, Korea University, Seoul 02841, South Korea

[⊥]School of Electrical Engineering, Korea University, Seoul 02841, South Korea

[∥]Division of Advanced Materials, Korea Research Institute of Chemical Technology, Daejeon 34114, South Korea

[#]High-Temperature Energy Materials Research Center, Korea Institute of Science and Technology, Seoul 02792, South Korea

[¶]Department of Nanomaterials Science and Technology, Korea University of Science and Technology, Daejeon 34113, South Korea

[⊗]Department of Materials Science and Engineering, Seoul National University of Science and Technology, Seoul 01811, South Korea

Supporting Information

ABSTRACT: Two-dimensional (2-D) metal chalcogenides have received great attention because of their unique properties, which are different from bulk materials. A challenge in implementing 2-D metal chalcogenides in emerging devices is to prepare a well-crystallized layer over large areas at temperatures compatible with current fabrication processes. Tin monosulfide, a *p*-type layered semiconductor with a high hole mobility, is a promising candidate for realizing large-area growth at low temperatures because of its low melting point. However, tin sulfides exist in two notable crystalline phases, SnS and SnS_2. Therefore, it is imperative to control the oxidation state of Sn to achieve a pure SnS film. Here, the synthesis of SnS thin films by atomic-layer-deposition (ALD) is demonstrated using bis(1-dimethylamino-2-methyl-2-propoxy)tin(II) and H_2S as Sn and S sources, respectively, over a wide temperature window (90−240 °C). Impurities such as carbon, oxygen, and nitrogen were negligibly detected. The morphological evolution of plate-like orthorhombic SnS grains was observed above 210 °C. Moreover, properties of thin film transistors and gas sensors using SnS films as the active layers were investigated. The SnS ALD process would provide promising opportunities to exploit the intriguing properties of the 2-D metal chalcogenides for realizing emerging electronic devices.

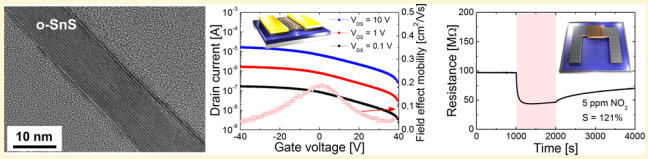

1. INTRODUCTION

Two-dimensional (2-D) metal chalcogenides have attracted immense interest in recent years, owing to their great potential for applications such as electronic switching devices and sensors.[1−5] In contrast to graphene, which has a zero band gap, the 2-D metal chalcogenides are characterized by a finite band gap. This allows high on/off current ratios in thin film transistors (TFTs) based on 2-D metal chalcogenides. The *n*-type and *p*-type semiconducting properties can also be selectively incorporated in devices, depending on the type of 2-D metal chalcogenide material.[6] Therefore, utilization of the 2-D metal chalcogenides could allow implementation of a *p*−*n* heterojunction, and further the realization of emerging devices such as complementary metal-oxide-semiconductor (CMOS) circuits.

Technical applications require techniques that enable the integration of the 2-D metal chalcogenides in emerging devices. One of the key techniques for implementing the 2-D metal chalcogenides in industrial applications is the synthesis of well-crystallized sheets over a large area, and many efforts have been devoted for this. Various techniques such as chemical vapor deposition,[7,8] atomic layer deposition (ALD),[9,10] and sulfurization of metals and metal oxides[11,12] have been introduced for the large-area synthesis of representative 2-D metal chalcogenides such as MoS_2 and WS_2. Despite significant progress in the growth of high-quality MoS_2 and WS_2 layers using these processes, they are generally performed at very high temperatures (>800 °C), which are not compatible with conventional electronic device fabrication processes.

SnS is an intrinsic *p*-type layered semiconductor with an indirect band gap of 1.0 to 1.1 eV in orthorhombic crystal structure.[13] Bulk SnS shows high hole mobilities of 500 and 90

Received: May 5, 2017
Revised: September 12, 2017
Published: September 13, 2017

DOI: 10.1021/acs.chemmater.7b01856
Chem. Mater. 2017, 29, 8100−8110

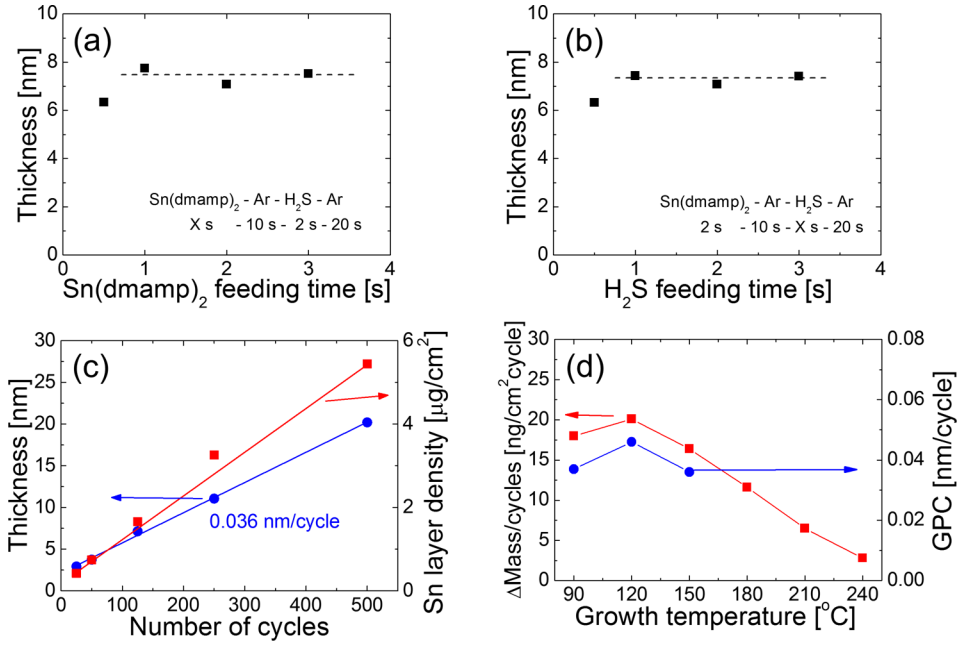

Figure 1. Variation in the thickness of the films grown at 150 °C over 125 cycles as a function of (a) $Sn(dmamp)_2$ and (b) H_2S feeding times. (c) The variation in the thickness and Sn layer density of SnS films grown at 150 °C as a function of the cycle number. (d) The variation in the GPC and mass gain per cycle of the SnS films as a function of the growth temperature.

cm^2/V s along the parallel and perpendicular directions of the interlayers, respectively.[14] Therefore, SnS could be a promising candidate for a *p*-type channel in electronic devices. More importantly, the melting point (T_m) of SnS is only 882 °C, much lower than those of MoS_2 (1185 °C) and WS_2 (1250 °C). The low T_m of SnS renders the growth of high-quality SnS film at relatively low temperature probable, which would be largely beneficial for their integration in current electronic devices.

However, tin sulfides exist in two notable forms, SnS (orthorhombic structure) and SnS_2 (hexagonal structure). It has been challenging to synthesize the SnS single phase without the formation of the other phase, mainly because +4 oxidation state of Sn is more stable than +2, which renders SnS_2 more stable. Therefore, a careful control of the growth conditions is necessary to achieve phase-pure SnS films. There are only limited reports on the growth of orthorhombic 2-D SnS. Mutlu et al. reported the growth of tin sulfides via a vapor-phase method,[15] and discovered that SnS was formed at a lower temperature of 425 °C while SnS_2 grew at 550 °C.[15] Yang et al. also reported that the growth temperature is a key factor in determining the crystal phase of tin sulfides in the sulfurization of Sn metal films.[16] However, according to their study, the temperature window for the growth of pure SnS is very narrow compared to that of SnS_2.[16] Ham et al. reported ALD of SnS_x thin films from tetrakis(dimethylamino)tin precursor which contains Sn in the +4 oxidation state,[17] and the phase of the ALD-grown SnS_x films was reported to change from hexagonal SnS_2 at the intermediate temperatures of 140−150 °C to orthorhombic SnS at temperatures of 160−180 °C.[17] The narrow temperature range for obtaining the SnS phase is understandable considering the +4 oxidation state of the Sn precursor. Even for the case of using a Sn precursor with +2 Sn oxidation state, Browning et al. reported that the ALD using tin(II) acethylacetonate and H_2S formed a mixed phase of SnS and SnS_2 below 250 °C, whereas a pure SnS film was formed at 300 °C.[18]

There have been recently more and more studies on ALD of metal sulfides using H_2S as the S source.[19−22] In this work, growth of pure SnS films was attempted via an ALD technique, using bis(1-dimethylamino-2-methyl-2-propoxy)tin(II) (Sn-$(dmamp)_2$) as the Sn precursor, in which Sn is in +2 oxidation state, and H_2S as the S source. The +2 oxidation state of Sn significantly influenced the growth of the impurity-free SnS phase over a relatively wide temperature window of 90−240 °C. TFT and interdigitated electrode (IDE) patterns were also fabricated utilizing the ALD-grown SnS films, and their electrical performance was characterized toward their potential applications in CMOS and gas sensors. The low-temperature ALD process would enable the practical use of *p*-type SnS in fabrication processes for emerging electronic devices with a stringent thermal limit.

2. RESULTS AND DISCUSSION

The authors previously studied the ALD growth of both *p*-type SnO and *n*-type SnO_2 using $Sn(dmamp)_2$ as the Sn precursor[23−25] and reported that the use of H_2O and O_3 as the oxygen source in ALD resulted in the formation of SnO and SnO_2 below a growth temperature of 230 °C, respectively.[23,24] However, the ALD chemistry with $Sn(dmamp)_2$ for tin sulfide growth has not been comprehensively investigated so far. Therefore, the self-saturation behavior of the ALD reaction from $Sn(dmamp)_2$ and H_2S was examined. Figure 1a,b shows the variation in the thickness of the films grown on SiO_2/Si at 150 °C for 125 cycles, as a function of $Sn(dmamp)_2$ and H_2S feeding times, respectively. The film thickness saturates at approximately 7 nm with the increase in both $Sn(dmamp)_2$ and H_2S feeding times. This suggests that the tin sulfide growth from $Sn(dmamp)_2$ and H_2S relies on a self-limiting ALD reaction. A similar self-saturation behavior in the ALD reaction of SnO films using an identical Sn precursor and H_2O has been

DOI: 10.1021/acs.chemmater.7b01856
Chem. Mater. 2017, 29, 8100−8110

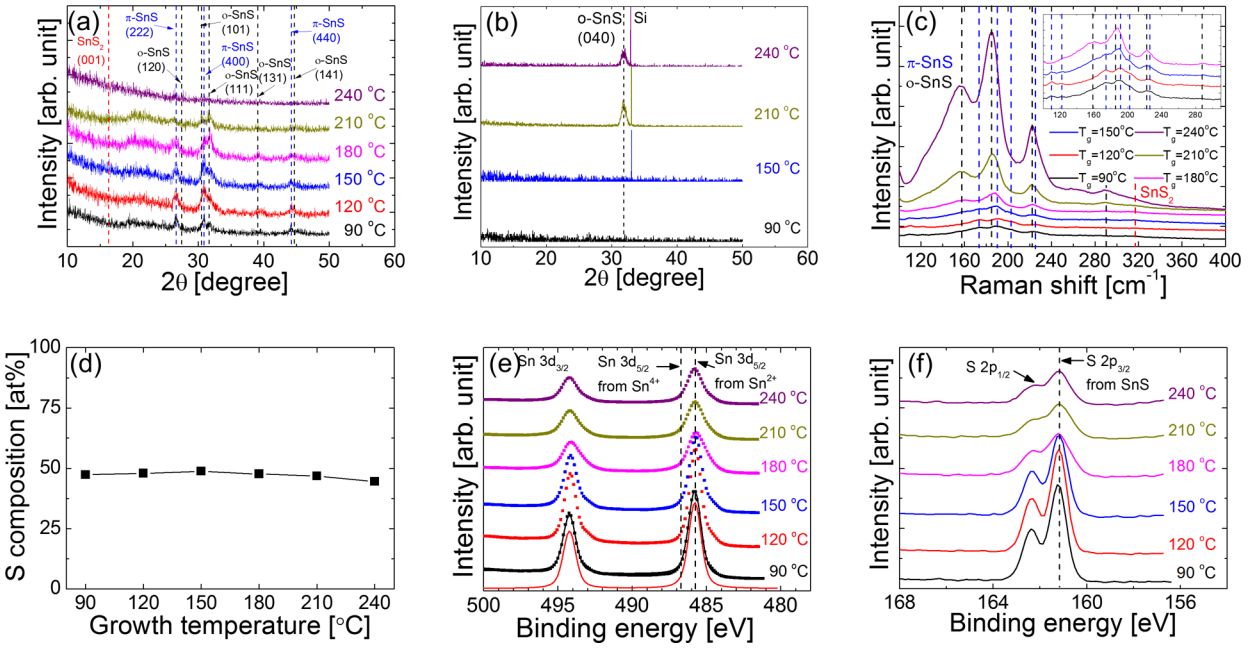

Figure 2. (a) 2θ XRD, (b) θ–2θ XRD, and (c) Raman spectra of the films grown in the temperature range from 90 to 240 °C. (d) Variation in the [S]/[Sn+S] atomic ratio of the films evaluated by WDXRF, as a function of the growth temperature. XPS spectra of (e) Sn 3d and (f) S 2p core levels in the films grown in the temperature range of 90–240 °C. The layer density of the films are 4.5 $\mu g/cm^2$ (250 cycles) at 90 °C, 5.0 $\mu g/cm^2$ (250 cycles) at 120 °C, 4.1 $\mu g/cm^2$ (250 cycles) at 150 °C, 2.9 $\mu g/cm^2$ (250 cycles) at 180 °C, 1.8 $\mu g/cm^2$ (280 cycles) at 210 °C, and 0.8 $\mu g/cm^2$ (300 cycles) at 240 °C, respectively.

reported.[23,25] Interestingly, the ALD reaction of the SnO films required a long H_2O feeding time (>5 s) while the saturation in the ALD reaction with H_2S in the current work was observed at a much shorter H_2S feeding time of 1 s. Notably, the amount of H_2O vapor (~3 × 10^7 Langmuir) required for self-saturation was much larger than that of H_2S (~1.8 × 10^5 Langmuir) used in this work. Considering the enormous difference in the required amounts of different precursors for self-saturation, it is presumed that the chemical reaction in ALD from the $Sn(dmamp)_2$ and H_2S precursors is more active than in ALD from $Sn(dmamp)_2$ and H_2O precursors.

Figure 1c shows the variation in the thickness of the SnS films grown at 150 °C as a function of the number of cycles. The film thickness is directly proportional to the number of cycles, exhibiting an excellent control over the thickness. The GPC calculated from the slope of the graph is approximately 0.036 nm/cycle at the growth temperature of 150 °C. Although the plot of the film thickness versus the number of cycles shows a *y*-intercept of approximately 2 nm, the *y*-intercept does not seem to result from the fluent initial growth. Figure 1c also shows the variation in the Sn layer density of the films measured by wavelength dispersive X-ray fluorescence (WDXRF) as a function of the number of cycles. This plot shows a negligible *y*-intercept in contrast to the plot of the film thickness versus the number of cycles. The positive *y*-intercept in the plot of the film thickness versus the number of cycles is likely induced by the error in the film thickness measurement from ellipsometry at thicknesses less than 5 nm. The temperature dependence of the growth per cycle (GPC) was examined in the temperature range of 90 to 240 °C (Figure 1d). The variation in the mass gain per cycle, calculated from WDXRF measurements on SnS films grown over 250–300 cycles, yields a maximum value of ~20 ng/cm^2·cycle at 120 °C; and the mass gain per cycle decreases with increasing growth temperature, down to ~3 ng/cm^2·cycle at 240 °C. The variations in the thickness GPC values calculated from spectroscopic ellipsometry follow a similar trend up to 150 °C. The thickness evaluated from spectroscopic ellipsometry was not reliable for the films grown at temperatures above 150 °C, because of the surface roughening and partial coverage. The surface morphology of the grown films is discussed later.

Grazing incidence X-ray diffraction (GIXRD) was used to determine the crystalline phase of the tin sulfide films and the θ–2θ XRD scan was also performed to identify the preferential orientation of the SnS interlayer, parallel to the substrate. Figure 2a,b shows the (a) GIXRD and (b) the θ–2θ XRD spectra of the films grown at temperatures ranging from 90 to 240 °C, respectively. The corresponding film thickness was controlled in the range of 8–12 nm. Only SnS peaks are observed in both the GIXRD and θ–2θ XRD spectra, with no peaks corresponding to SnS_2 or Sn_2S_3. The SnS peaks are observed even in the 2θ spectra of the SnS films grown at the lowest temperature of 90 °C. This suggests that the crystallization of the SnS films occurs during the ALD process even at such low temperatures. Interestingly, two SnS phases, orthorhombic and cubic, are observed in the GIXRD spectra of the SnS films. Orthorhombic SnS (PDF 039-0354) has been mostly observed for SnS films grown by a wide range of methods.[26–28] The recently reported cubic π SnS phase has a lattice constant of 11.59 Å, which is nearly twice that of the zinc blende SnS structure.[29–32] Peaks corresponding to the (222), (400), and (440) planes of the cubic π phase are observed in the GIXRD spectra. The peak intensity of the crystal planes of the cubic phase decreases with increasing growth temperature, whereas the orthorhombic phase prevails at higher temperatures. However, no observation of any diffraction peak in the GIXRD pattern of the film grown at the highest temperature of 240 °C was quite extraordinary, but the film shows a strong (040) orthorhombic SnS peak in the θ–2θ XRD spectra (Figure 2b). This implies that the evolution of the single SnS

DOI: 10.1021/acs.chemmater.7b01856
Chem. Mater. 2017, 29, 8100–8110

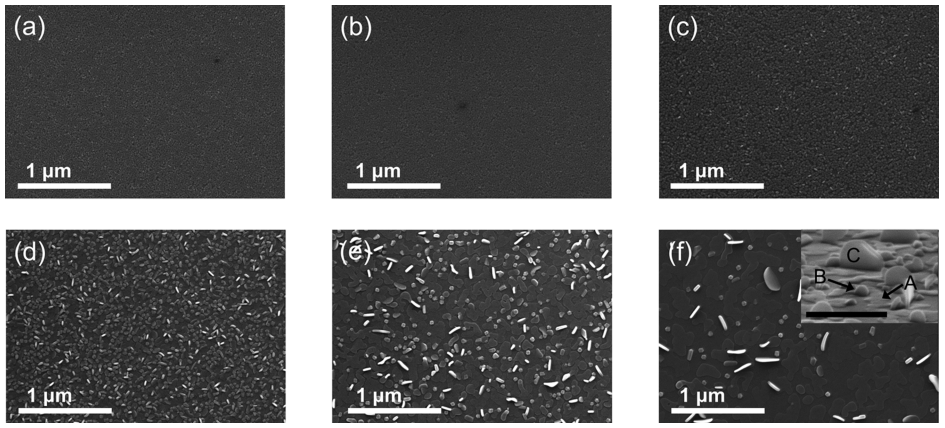

Figure 3. SEM plan-view images of the SnS films grown at (a) 90, (b) 120, (c) 150, (d) 180, (e) 210, and (f) 240 °C over 250−300 cycles. The inset in panel f shows the tilt SEM image of the SnS film grown at 240 °C. (Scale bar: 500 nm) A, B, and C in the inset indicate grains with a flat surface parallel to the substrate, 40−50 nm sized islands, and vertically grown plate-shaped grains, respectively.

phase with the van der Waals interlayers aligned parallel to the substrate is more dominant at higher temperatures of >210 °C. The SnS films grown at 90−150 °C do not show any peaks in the θ−2θ XRD spectra (Figure 2b), whereas the GIXRD spectra show crystalline SnS peaks. The XRD analysis reveals that the films grown at lower temperatures (less than ∼180 °C) are composed of relatively randomly oriented small grains while the films grown at higher temperatures (>210 °C) tend to have larger orthorhombic SnS grains with a preferential alignment of the (0k0) plane parallel to the substrate.

Because XRD could be insensitive to the presence of small amounts of Sn_2S_3 and SnS_2, Raman spectroscopy was used to further examine the possible presence of such minor phases. This technique has been reported to be much more sensitive to traces of these phases.[33] The Raman spectra displayed in Figure 2c show distinct characteristic Raman peaks at 158 (B_{3g}), 185 (A_g), 222 (A_g), and 290 cm^{-1} (B_{2g}), assigned to Raman modes of orthorhombic SnS, especially for the films grown at higher temperatures. The peak positions in the Raman shifts are consistent with those previously reported for orthorhombic SnS.[27,34,35] The films grown at the low temperatures of 90−150 °C show weak intensities of the peaks, which could be ascribed to the low crystalline quality of the films. The magnified spectra (inset in Figure 2c) clearly reveal that the films grown at these low temperatures consist of orthorhombic and cubic SnS phases. In addition to the Raman peaks of the orthorhombic SnS, the films show distinct characteristic Raman peaks at 110, 122, 174, 190, 203, and 225 cm^{-1}, corresponding to cubic π SnS, which is consistent with previously reported results for cubic π SnS.[30,32] The cubic π SnS phase is dominant at lower temperature, whereas higher temperatures favor the orthorhombic SnS phase, which is consistent with the XRD results shown in Figure 2a,b. A Raman peak at 315 cm^{-1}, which can be assigned to the A_{1g} mode of SnS_2,[15] is not observed in any of the Raman spectra shown in Figure 2c. It should be noted that the layer density of the films generally decreases with increasing growth temperature. The peak intensity of the Raman modes increases with increasing growth temperature, implying that the ALD growth at higher temperature yields well-crystallized large orthorhombic SnS grains, consistent with the XRD data presented in Figure 2b.

The [S]/[Sn+S] atomic ratios of the films were further evaluated by WDXRF, and the values were found to be close to 50% over the entire temperature range (Figure 2d). This finding further supports the formation of a single SnS phase by the ALD process. To further verify the oxidation state of the ALD-grown films, X-ray photoelectron spectroscopy (XPS) was carried out. Figure 2e,f shows the variations in the XPS spectra of Sn 3d and S 2p core levels, respectively, in the films grown at temperatures of 90−240 °C. The peak positions were calibrated using the adventitious C 1s signal (284.8 eV). The Sn $3d_{5/2}$ peak in the Sn 3d spectra of all the films is observed only at 485.7 eV, corresponding to the Sn oxidation state of +2. No peak corresponding to the +4 oxidation state of Sn (at 486.7 eV) is observed in Figure 2e. For easy comparison, the Sn spectra of the film grown at 90 °C were deconvoluted and were well fitted with just the Sn^{2+} peak. The S 2p spectra in Figure 2f also shows a single S $2p_{3/2}$ peak at 161.2 eV, which corresponds to the Sn−S bond of SnS. These XPS results are also consistent with the phase identification from the XRD, Raman, and WDXRF analyses. However, the intensities of the peaks in the Sn 3d and S 2p spectra significantly decrease above a growth temperature of 180 °C. As all the test films are >8 nm in thickness, which is larger than the typical probing depth of XPS, the decrease in the peak intensities cannot be due to the thinness of the films grown at higher temperatures. Rather, this decrease in the intensity could be related to the partial coverage of the SnS layer on the substrate at higher temperatures, as discussed later.

The optical band gap of the films grown at 90−150 °C, evaluated from the Tauc plot of the optical absorption spectra, is 1.45 eV, irrespective of the growth temperature (Figure S1, Supporting Information (SI)), whereas the reported band gap of SnS_2 is ∼2.2 eV. The measured band gap of the ALD-grown films is consistent with the value reported for SnS films from other studies,[16,27] which also corroborates the absence of Sn_2S_3 and SnS_2 phases in the ALD-grown films.

These findings suggest that the specific ALD chemistry adopted in this work facilitates the growth of pure SnS films over a wide temperature range, which is in stark contrast to the previous studies, in which the phase of the SnS_x films grown by other techniques were found to be strongly dependent on the growth temperature.[15,17,18,36] Such a critical merit of this specific ALD process can be attributed to the use of the Sn precursor with a +2 oxidation state. Sinsermsuksakul et al. also reported the growth of SnS films in ALD using Sn(MeC(N-iPr)$_2$)$_2$, a Sn(II) precursor.[27] In addition, the authors reported that a similar result could be achieved in the ALD of the

DOI: 10.1021/acs.chemmater.7b01856
Chem. Mater. 2017, 29, 8100−8110

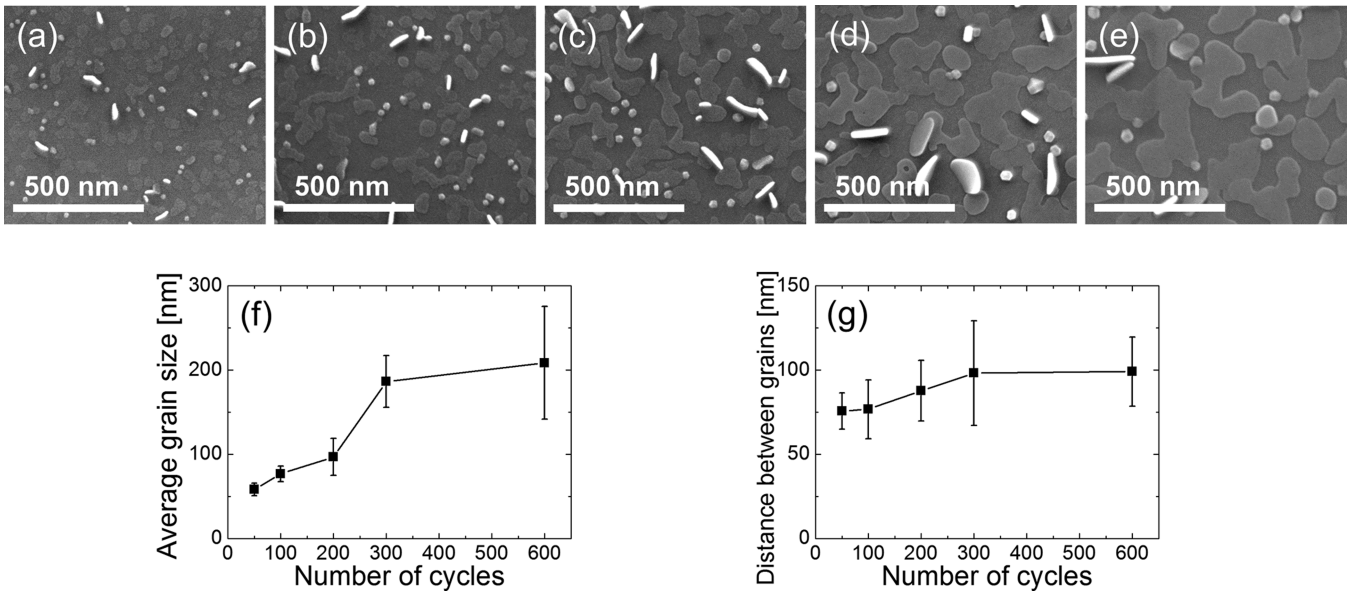

Figure 4. SEM plan-view images of the SnS films grown at 240 °C over (a) 50, (b), 100, (c) 200, (d) 300, and (e) 600 cycles. The variations in the (f) average grain size and (g) average distance between adjacent grains in the SnS films grown at 240 °C as a function of the cycle number.

metastable SnO phase using an identical Sn-precursor and H_2O.[23,25]

Figure 3a–f shows the scanning electron microscopy (SEM) images of the SnS films grown at (a) 90 (250 cycles, layer density of SnS: 4.5 $\mu g/cm^2$), (b) 120 (250 cycles, 5.0 $\mu g/cm^2$), (c) 150 (250 cycles, 4.1 $\mu g/cm^2$), (d) 180 (250 cycles, 2.9 $\mu g/cm^2$), (e) 210 (280 cycles, 1.8 $\mu g/cm^2$), and (f) 240 °C (300 cycles, 0.8 $\mu g/cm^2$), respectively. The surfaces of the films grown at 90 and 120 °C are apparently smooth (root-mean-squared roughness of the two films estimated by atomic force microscopy is ∼1 nm; Figure S2, SI). However, the surface morphology of the SnS film is drastically roughened with the increase in the growth temperature above 150 °C. Moreover, the substrate surface was not fully covered with the SnS layers at higher growth temperatures. The Si 2p XPS peak assigned to SiO_2, the substrate, is also observed in the films grown above 180 °C (Figure S3, SI), confirming the partial coverage of SnS on the SiO_2 substrate, as shown in Figure 3e,f. Interestingly, three different types of grain shapes, grains with a flat surface parallel to the substrate (type A), 40–50 nm sized islands (type B), and vertically grown plate-shaped grains (type C) are observed in the films grown above 180 °C. The tilt SEM image in the inset of Figure 3f clearly exhibits the morphology of these three types of grains. The appearance of the plate-shaped grains is a unique characteristic in the growth of layered 2-D materials.[8,37−40] In general, an anisotropic shape is developed in the synthesis of layered materials because the adsorption of the materials on the van der Waals surface is not favored, while the adsorption on the edges with a large number of dangling bonds is enhanced. Moreover, the development of the plate-shaped SnS grains parallel to the substrate surface prevails at the high growth temperature of 240 °C over other types of grains. The average size of the plate-shaped SnS grains also increases with increasing growth temperature. The emergence of a (040) SnS peak in the θ–2θ XRD spectra and the strong intensities of the SnS peaks in the Raman spectra of the SnS film grown at 240 °C (Figure 2) can be rationalized by the development of the plate-shaped orthorhombic SnS large grains arranged parallel to the substrate.

Interestingly, the vertically arranged SnS plates are longer than 100 nm (Figure 3f). Considering the low GPC at 240 °C and short cycles (300 cycles) which would induce a low corresponding film thickness of only <5 nm, the formation of such large SnS plates are not expected in the normal ALD growth of SnS films. Therefore, to further explore the possible origins of the development of these large plates, the surface morphology of the SnS films was examined as a function of the number of cycles. Figure 4a–e shows the SEM images of the SnS films grown at 240 °C over (a) 50, (b), 100, (c) 200, (d) 300, and (e) 600 cycles, respectively. In the beginning, discrete islands with plate-like shapes parallel to the substrate are formed, and the lateral size of the plate-shaped SnS grains arranged parallel to the substrate increases with increasing number of cycles, while a significant portion of the substrate surface (SiO_2 film) remains uncovered even for a high cycle number of 600. For a quantitative comparison, the lateral size of the SnS grains was estimated by an intercept method. Figure 4f shows the average grain size of the SnS grains in the films grown at 240 °C with respect to the number of cycles. The lateral size of the SnS grains arranged parallel to the substrate is approximately 50 nm even for a low cycle number of 50 and the size is significantly increased to ∼180 nm after 300 cycles. The lateral growth per cycle in the cycle range is as large as 0.5 nm/cycles, which is approximately 40 times larger than the overall GPC (∼0.012 nm/cycle) of the film estimated from the mass gain per cycle at this temperature (Figure 1d). After the formation of the SnS nuclei, if the active adsorption on the edge of the SnS nuclei is the origin of the rapid lateral growth, the distance between the adjacent grains should decrease significantly with increasing number of cycles. Therefore, the distance between the adjacent grains was also compared in a regime where the SnS continuous film had not formed. Figure 4g shows the variation in the average distance between the adjacent SnS grains with respect to the number of cycles. Interestingly, the distance between the adjacent SnS grains slightly increases from 75 nm at the 50th cycle to 100 nm at the 600th cycle. It should be noted that, as shown in Figure 4f the average grain size in the films grown at 240 °C significantly

DOI: 10.1021/acs.chemmater.7b01856
Chem. Mater. 2017, 29, 8100−8110

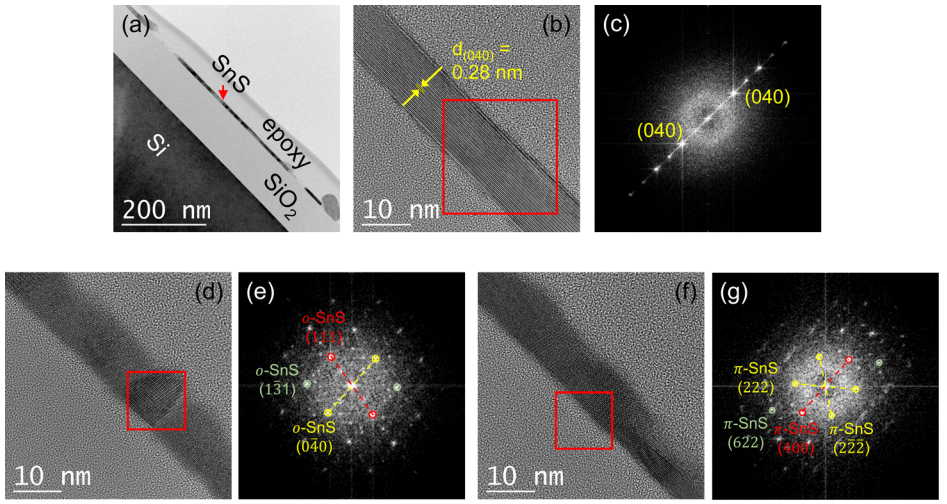

Figure 5. (a) Low-magnification TEM and (b) HRTEM images of the SnS film grown at 240 °C. (c) FFT image corresponding to the red box in panel b. (d and f) HRTEM images of the SnS film grown at 90 °C. (e and g) FFT images corresponding to the red boxes in panels d and f, respectively.

increased from approximately 50 nm at 50 cycles to approximately 200 nm at 600 cycles. Therefore, it can be concluded that the substantial lateral growth at the high temperature of 240 °C is mainly owing to the coalescence by a facile migration of the adsorbed SnS, not the selective adsorption of the SnS to the edges of plates. This is also supported by the absence of small plate-like grains of 40−50 nm in size, observed at the initial growth stage in the film grown over 600 cycles (Figure 4e). If the adsorbed SnS grains did not migrate during the growth, SnS nuclei should be formed on the area of the surface not covered by the SnS grains.

The facile migration and coalescence during the film growth was not expected at such low temperatures (<250 °C). However, it is noteworthy that the adatom mobility is related to the reduced growth temperature (T/T_m) rather than only the growth temperature.[41−43] In this work, T/T_m for the growth of SnS is 0.44 at a growth temperature of 240 °C, which is much larger than the values for other common materials fabricated by ALD: T/T_m is equal to 0.25 for TiO_2, 0.23 for ZnO, and only 0.17 for HfO_2 when the ALD temperature was fixed at 250 °C. The corresponding growth temperatures for these materials at the same T/T_m of 0.44 are as high as 660 °C for TiO_2, 716 °C for ZnO, and 1060 °C for HfO_2. This suggests that the high T/T_m in this SnS ALD could result in the rapid lateral growth of SnS through coalescence by the easy migration of the adsorbed SnS.

High-resolution transmission electron microscopy (HRTEM) was used to further understand the structure of the grown SnS films. Figure 5a,b shows the TEM images of the SnS film grown at 240 °C. The low-magnification TEM image in Figure 5a verifies the formation of noncontinuous and very large SnS grains. The HRTEM image in Figure 5b shows the planes with an interspacing of 0.28 nm that corresponds to orthorhombic (040) planes. The fast Fourier transform (FFT) image (Figure 5c) corresponding to the red box in Figure 5b also verifies the layered structure of the SnS. The cubic SnS phase was not observed in the TEM analysis of the film grown at 240 °C. This HRTEM analysis also indicates that the van der Waals interlayers of the orthorhombic SnS are well aligned parallel to the substrate for the film grown at 240 °C, which is consistent with the XRD results shown in Figure 2b.

Figure 5d,f shows the HRTEM images of the SnS film grown at the lowest temperature of 90 °C. In contrast to the film grown at 240 °C, a continuous film grew at 90 °C and the film was composed of randomly oriented small SnS grains (lateral size: ∼10 nm). To further elucidate the crystal structure of the grains, FFT images were taken of the selected area. Figure 5e,g shows the FFT images corresponding to the red box in Figure 5d,f, respectively. The analyses of the reciprocal lattice points in Figure 5e,g revealed that the corresponding SnS grains had orthorhombic and cubic π SnS structures, respectively. This result indicates the formation of mixed orthorhombic and cubic SnS phases at lower temperatures, and it coincides the XRD and Raman results shown in Figure 2a,c, respectively.

The $Sn(dmamp)_2$ precursor has oxygen and carbon in the molecule. Therefore, their residues that may remain in the films were investigated by XPS. Indeed, Kim et al. reported a considerable oxygen residue of ∼20% in the SnS films grown by ALD from tin(II) 2,4-pentanedionate ($Sn(acac)_2$) and H_2S.[44] Figure 6a,b shows the XPS spectra of O 1s and C 1s core levels,

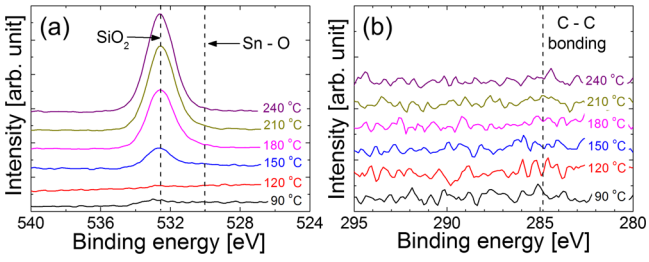

Figure 6. XPS spectra of (a) O 1s and (b) C 1s core levels for the SnS films grown in the temperature range from 90 to 240 °C after short Ar sputtering to remove surface contaminants.

respectively, for the SnS films after short Ar sputtering in the XPS chamber to remove surface contaminants. While the films grown at 90 and 120 °C do not exhibit any peak in the O 1s XPS spectra, the films grown above 150 °C show a peak at 532.5 eV (Figure 6a). However, the observed O 1s peaks correspond to Si−O bond originating from the carbonyl or

DOI: 10.1021/acs.chemmater.7b01856
Chem. Mater. 2017, 29, 8100−8110

hydroxyl groups adsorbed on the surface and SiO_2 substrate, and not to the Sn−O bond. The occurrence of the peak from the substrate could be partly owing to the film thickness (less than the effective escape depth of photoelectrons) after the short Ar sputtering but mostly from the partial coverage of SnS on the SiO_2 substrate at higher growth temperatures, as shown in Figure 4. No peak at 530 eV, corresponding to Sn−O bond, is observed for the films grown over the entire temperature range. Moreover, no peak is observed in the C 1s XPS spectra (Figure 6b). The impurity contents in the SnS films were further confirmed by Auger electron spectroscopy (AES). The AES analysis also confirms that the ALD-grown SnS films contain negligible oxygen and nitrogen contents (Table 1).

Table 1. Oxygen and Nitrogen Impuritis in the SnS Films Grown at 90, 120, and 150 °C, Determined by AES

	Growth temperature [°C]		
Element [%]	90	120	150
Oxygen	Not detected	0.9	2.3
nitrogen	Not detected	Not detected	0.1

These results demonstrate that the ALD process from $Sn(dmamp)_2$ and H_2S could be a feasible technique to obtain pure SnS films with respect to impurity concentration and phase purity, even with the stringent thermal limit of <250 °C.

The ALD of SnS films was also carried out on Al_2O_3-coated SiO_2/Si (4 nm-thick Al_2O_3 was grown by ALD at 150 °C, using $Al(CH_3)_3$ and H_2O) substrate and the results are compared with those on the SiO_2 surface. Figure 7a,b shows the variation in the Sn layer density of the SnS films grown on SiO_2 and Al_2O_3 at 90 and 240 °C, respectively, as a function of the number of cycles. At 90 °C, the growth of SnS on Al_2O_3 is severely retarded at the initial growth stage and is recovered above 250 cycles while the ALD of SnS on SiO_2 shows negligible retardation. The SEM images of the films grown at 90 °C (Figure 7c) reveal a dense nucleation of SnS on the SiO_2 surface, thereby resulting in the formation of continuous SnS films already in the initial cycles. However, only sparse nuclei are observed on the Al_2O_3 in the early stages of the film growth, and almost full coverage via coalescence of the nuclei could be achieved only at a long cycle number of 600 (Figure 7d). At 240 °C, the substrate-dependent film growth behavior was much more pronounced. Although the GPC at 240 °C is lower than that at 90 °C, the Sn layer density of SnS on SiO_2 appears to increase linearly from the initial cycle (Figure 7b). On the other hand, the SnS growth did not occur on Al_2O_3 at 240 °C even for a long cycle number of 600. This demonstrates that the ALD from $Sn(dmamp)_2$ and H_2S shows a strong substrate dependency. Further study on such substrate dependency will be reported elsewhere.

SnS TFTs were fabricated on a 100 nm-thick SiO_2 gate insulator to characterize the electrical properties of the ALD-grown SnS. Figure 8a shows the schematic of the fabricated SnS TFTs. The TFT with a 10 nm-thick SnS film grown at 150 °C shows typical *p*-type transfer behavior and an on/off current ratio of 60, (Figure S4, SI) which is larger than the values (1.5 from 30 nm-thick SnS grown above 600 °C[45] and 20 from 50 nm-thick SnS annealed at 400 °C)[46] obtained for SnS fabricated by other techniques. Yet, the device did not show a promising TFT performance (the device did not fully turn off even at a very high positive gate voltage of 40 V), and the estimated field effect mobility is as low as 6×10^{-5} $cm^2/(V\ s)$. This low mobility might result from the small SnS grains and point defects within these small-sized grains, where the serious grain boundary (and defect) scattering prohibits the facile carrier transport. This hypothesis invokes that the SnS film grown at 240 °C, which has a much larger grain size and higher crystallinity, may show a better TFT performance. However, TFTs with the SnS film grown at 240 °C did not show any significant current transport even under the accumulation condition (−40 V gate voltage), which might be ascribed to the

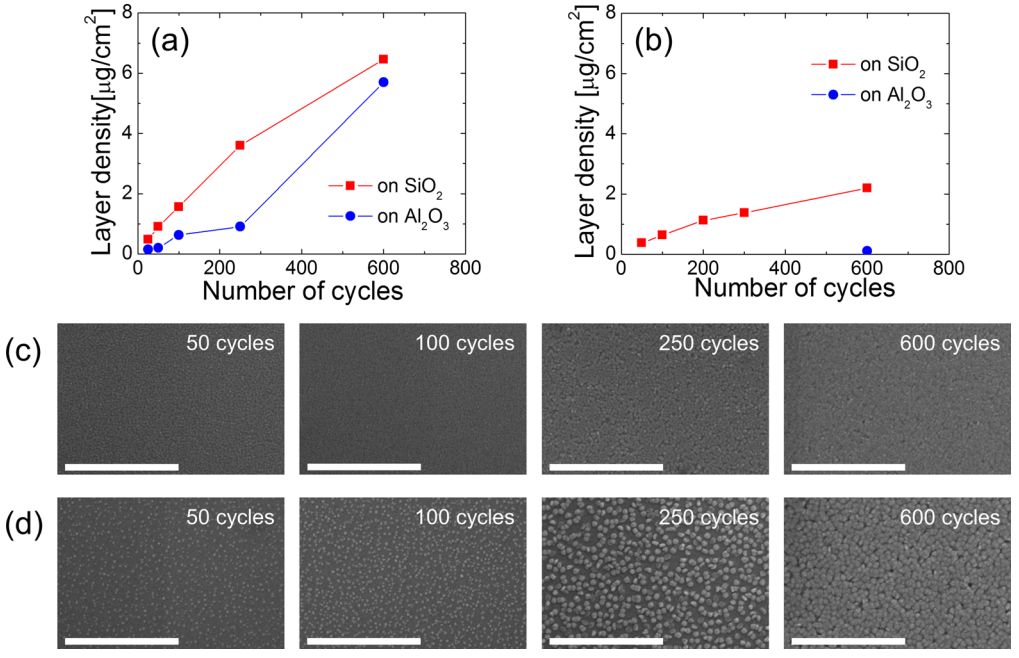

Figure 7. Sn layer density of the SnS films grown on SiO_2 and Al_2O_3 surfaces at (a) 90 and (b) 240 °C as a function of the number of cycles. SEM plan-view images of the films grown at 90 °C on (c) SiO_2 and (d) Al_2O_3 over 50, 100, 250, and 600 cycles. (Scale bar: 500 nm).

DOI: 10.1021/acs.chemmater.7b01856
Chem. Mater. 2017, 29, 8100−8110

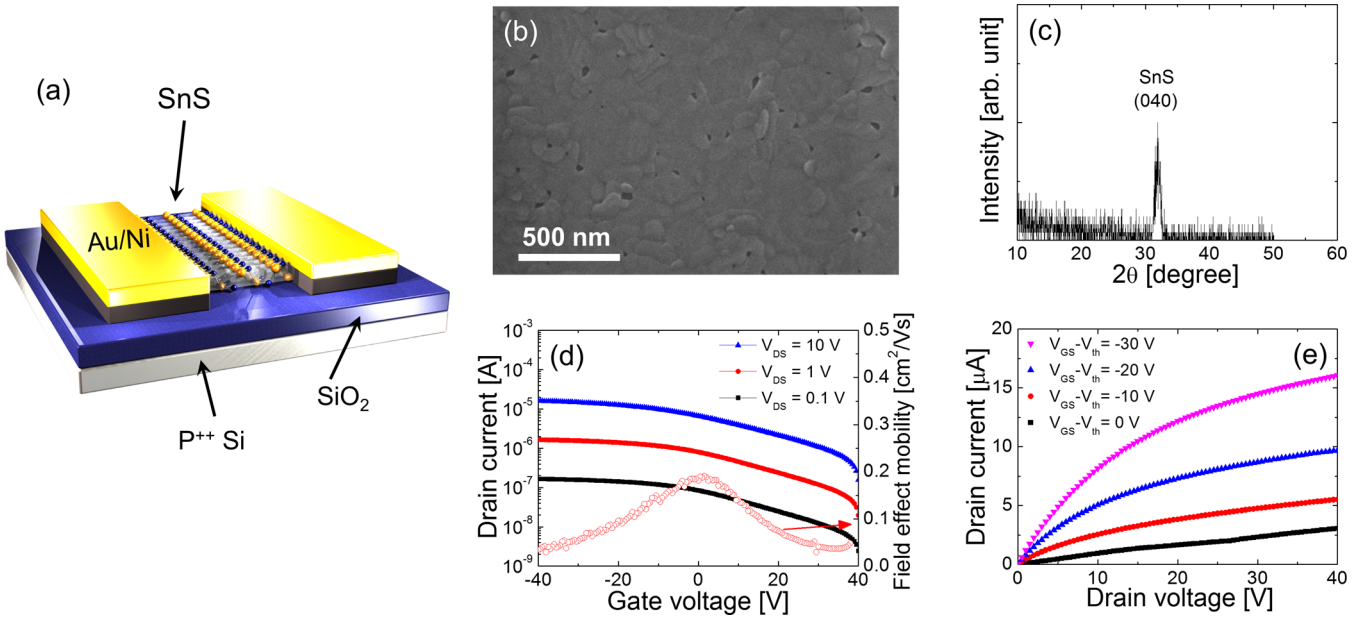

Figure 8. (a) Schematic of the SnS bottom-gate TFT. (b) SEM image and (c) XRD spectra of a SnS film grown via the two-step ALD growth. (d) Transfer curves and (e) output characteristics of the TFT.

discontinuous SnS film grains. To resolve the issue, a thin and continuous SnS film was grown at 90 °C over 250 cycles and additional growth of SnS at 240 °C over 350 more cycles was performed (two-step process). The thickness of the film formed by the two-step process is approximately 12 nm. Figure 8b shows the SEM image of this SnS film, revealing the formation of a continuous film with relatively large SnS grains. The θ–2θ XRD spectra in Figure 8c confirm that the van der Waals layer in the SnS film is well-aligned parallel to the surface. The Hall measurement reveals that the film shows a *p*-type conduction, and the estimated Hall mobility is approximately 2.9 $cm^2/(V\,s)$. Figure 8d displays the transfer curves of the TFT with the SnS layer grown by the two-step process, showing a typical *p*-type conduction behavior. The output characteristics shown in Figure 8e reveal a typical *p*-type conduction behavior as well. The field effect mobility is estimated to be approximately 0.18 $cm^2/(V\,s)$, which is much larger than that of the TFT with SnS grown at 150 °C. The on/off current ratio of the TFT also improved to approximately 80, which is larger than the single layer data (Figure S4, SI) and also larger than the value (~10) obtained from TFTs utilizing exfoliated SnS of 50–100 nm.[47] Although the demonstrated device performance is slightly low compared to other *p*-type oxide TFTs (~1 $cm^2/(V\,s)$) based on common oxides such as SnO and CuO_x films,[25,48,49] these results demonstrate that the performance could be improved significantly by optimizing the microstructure of the SnS film through process optimization, including ALD process conditions and postdeposition annealing.

2-D metal chalcogenides have also attracted interest as functional materials for gas sensing. Although semiconducting metal oxides have been used as conventional chemical sensing materials, gas sensors based on metal oxides require high temperatures because of their low sensitivity at room temperature, resulting in severe power consumption issues. For the potential application of SnS films in low-power gas sensors, the sensing characteristics of the ALD-grown SnS film fabricated on Pt IDEs were examined. Figure 9a shows the schematic of the test sensor device with a SnS layer grown at 90

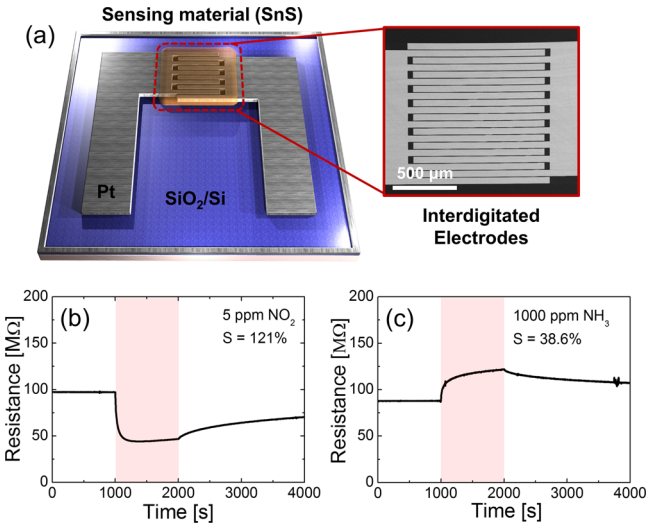

Figure 9. (a) Schematic of the SnS gas sensor and SEM image of the vicinity of the interdigitated electrodes. The variation in the resistance of the gas sensor composed of SnS grown at 90 °C under the exposure of two different gases, (b) 5 ppm of NO_2 and (c) 1000 ppm of NH_3, at room temperature. Red vertical bars indicate the target gas injection for 1000 s.

°C. Dynamic change in the resistance of the device was monitored under the exposure of two different gases, 5 ppm of NO_2 and 1000 ppm of NH_3, at room temperature. The resistance of the device decreased upon exposure to 5 ppm of NO_2 at 1000 s (Figure 9b), which is consistent with the electrical responses from other SnS gas sensors under similar change in the atmosphere.[50] NO_2 is known to act as an acceptor,[51] leading to increased hole concentration in the SnS layer upon its exposure to NO_2. When the NO_2 flow was stopped after 2000 s, the device slowly recovers its initial resistance, because of the desorption of the gaseous molecules from the SnS layer. In contrast, the resistance of the device increased upon exposure to 1000 ppm of NH_3 at 1000 s

DOI: 10.1021/acs.chemmater.7b01856
Chem. Mater. 2017, 29, 8100–8110

(Figure 9c). NH_3 adsorbed on layered materials acts as a donor. When the NH_3 gas flow was stopped after 2000 s, the device's resistance decreased to the initial value at a much slower rate and even after 2000 s, the initial value was not fully recovered. This is possibly due to numerous grain boundaries in the SnS film, which render the desorption of the adsorbed gas difficult. The sensitivity of the device (S) for negative and positive resistance responses is defined as $(R_a - R_g)/R_g$ and $(R_g - R_a)/R_a$, respectively, where R_a and R_g represent the resistance of the device under the exposure of air and the sensing gas, respectively. The S value of the SnS device at room temperature is 121% for 5 ppm of NO_2 and 38.6% for 1000 ppm of NH_3. This implies that the charge transfer mechanism operates in the SnS device even at room temperature probably through the physisorption of the target molecules on the SnS surface. In general, chemisorption is dominant at elevated temperatures, whereas physisorption is dominant at low temperatures because the activation energy of chemisorption is larger than that of physisorption.[52] In particular, 2-D materials such as SnS are not very chemically active because of the van der Waals nature of their interlayer bonding. This means that the target gas will only weakly interact with the surface via physisorption rather than via chemisorption.[53] This relatively high and different sensitivity of the SnS device for low concentrations of NO_2 and NH_3 at room temperature demonstrates that the ALD-grown SnS could be a promising candidate for low-power gas sensing with a high sensitivity.

3. CONCLUSION

The growth of p-type and impurity-free SnS films by ALD at low temperatures (90 to 240 °C) is demonstrated using $Sn(dmamp)_2$ and H_2S as the Sn and S precursors, respectively. Despite the stringent thermal limit of 240 °C, impurities such as carbon, oxygen, and nitrogen were negligibly detected in the SnS films, and no other phases such as Sn_2S_3 and SnS_2 were formed. The use of $Sn(dmamp)_2$, in which the oxidation state of Sn is +2, enables the formation of the SnS with a single Sn oxidation state of +2 and widens the ALD window for its growth. Although SnS films composed of cubic and orthorhombic mixed phases formed at lower temperatures, plate-like orthorhombic SnS grains are developed with their alignment parallel to the substrate surface prevails at higher growth temperatures of >210 °C. The lateral grain size of SnS increases with increasing growth temperature. The high mobility of the adatoms on the substrate surface, induced by the extremely high T/T_m (0.44 at 240 °C), leads to large lateral grain sizes and the evolution of noncontinuous films. Moreover, the ALD of SnS films shows different growth behaviors on SiO_2 and Al_2O_3 surfaces, suggesting that the adsorption of SnS is strongly dependent on the substrate type. The implementation of the ALD-grown SnS in TFTs and gas sensors confirmed the feasibility of their application in emerging devices. The development of the ALD process with the stringent thermal limit of <250 °C will lead to further exploration of facile routes to realize emerging electronic devices utilizing 2-D metal chalcogenides, at the industrial level.

4. EXPERIMENTAL SECTION

Film Growth. SnS thin films were grown in a traveling-wave type reactor via an ALD technique. $Sn(dmamp)_2$ was used as the Sn precursor. The $Sn(dmamp)_2$ precursor was synthesized in the laboratory. The detailed procedure on the synthesis of the precursor is reported elsewhere.[23,54] The canister containing $Sn(dmamp)_2$ was heated at 52 °C. The Sn precursor was delivered to the reactor with an Ar flow rate of 150 sccm. H_2S (3.5%)/Ar gas mixture at a flow rate of 400 sccm was used as the S precursor. The feeding time of each precursor was varied to investigate the self-saturation behavior. The feeding times of $Sn(dmamp)_2$ and H_2S were both fixed at 2 s after verification of the saturation behavior. After examination of the purging time of precursor, the purging times of $Sn(dmamp)_2$ and H_2S were fixed at 10 and 20 s, respectively, to prevent intermixing of these precursors. (Figure S5, SI) The growth temperature was varied from 90 to 240 °C. 100 nm-thick SiO_2/Si wafers were mainly used as the substrate. ALD-grown Al_2O_3/SiO_2/Si samples were used as the substrate to examine the influence of the substrate type on the growth behavior. Prior to the ALD growth, the substrates were cleaned by dipping them into acetone, ethanol, and deionized water for 5 min each. Note that H_2S gas is highly toxic and flammable.

Characterization. The thickness of the SnS film was determined by spectroscopic ellipsometry. As this technique was not appropriate for films grown at high temperatures, because of surface roughening, the extent of growth for the SnS films grown at higher growth temperatures was measured by WDXRF. The Sn/S ratio in the grown films was also obtained by the WDXRF analysis. The surface morphology of the SnS films was observed by SEM and atomic force microscopy. XRD (ATX-G, Rigaku) and Raman spectroscopy (inVia Raman Microscope, Reinshaw) were utilized to verify the phase of the grown films. The XRD measurements were carried out at a scan rate of 4°/min with an X-ray source of Cu Kα and the Raman observation was performed using a Nd:Yag laser (532 nm wavelength). The chemical analysis of the films was carried out by XPS (PHI 5000 VersaProbe, Ulvac-PHI) and AES (PHI 700, Ulvac-PHI). The XPS experiment was performed using a monochromatic X-ray source of Al Kα at a pass energy of 23.5 eV and a step size of 0.125 eV. The AES experiment was carried out using a field emission electron gun of 3 kV. Ar sputtering of 1 kV was used for the depth profile analysis. The microstructure and crystal structure of the films were examined by HRTEM (Titan TEM, FEI).

Device Fabrication. A bottom-gate TFT structure was used to characterize the electrical properties of SnS TFTs. Heavily doped p-type Si and 100 nm-thick SiO_2 served as the gate and gate insulator, respectively. The active channel was patterned by photolithography and etched by dry etching. Ni/Au pads were used as the source/drain electrodes. A 30 nm-thick Ni layer was grown by e-beam evaporation and subsequently, 30 nm-thick Au layer was grown by thermal evaporation in the same chamber without breaking the vacuum. The width and length of the active channel are 300 and 50 μm, respectively. For the fabrication of the SnS gas sensors, Pt IDEs were fabricated as shown in Figure 8a. A 100 nm-thick Pt layer was grown by e-beam evaporation and then the layer was patterned by photolithography. The distance between the interdigitated electrodes was fixed at 5 μm. SnS thin films were grown on Pt IDEs at 90 °C.

■ ASSOCIATED CONTENT

Supporting Information

The Supporting Information is available free of charge on the ACS Publications website at DOI: 10.1021/acs.chemmater.7b01856.

Additional information on purging time dependence of the thickness, Tauc plot, XPS, and AFM data of the SnS films and transport properties of the TFT with a SnO film grown at 150 °C (PDF)

■ AUTHOR INFORMATION

Corresponding Author

*S. K. Kim. E-mail: s.k.kim@kist.re.kr.

ORCID

Taek-Mo Chung: 0000-0002-5169-2671

Cheol Seong Hwang: 0000-0002-6254-9758

Seong Keun Kim: 0000-0001-8712-7167

DOI: 10.1021/acs.chemmater.7b01856
Chem. Mater. 2017, 29, 8100−8110

Notes

The authors declare no competing financial interest.

■ ACKNOWLEDGMENTS

This work was supported by the National Research Council of Science & Technology (NST) grant by the Korea government (MSIP) (No. PCS-17-02-KIST) and the Korea Institute of Science and Technology (KIST through 2E27120). C.S.H. acknowledges the support from the National Research Foundation of Korea through a grant (No. NRF-2014R1A2A1A10052979).

■ REFERENCES

(1) Radisavljevic, B.; Radenovic, A.; Brivio, J.; Giacometti, V.; Kis, A. Single-layer MoS_2 transistors. *Nat. Nanotechnol.* **2011**, *6*, 147−150.
(2) Wang, Q. H.; Kalantar-Zadeh, K.; Kis, A.; Coleman, J. N.; Strano, M. S. Electronics and optoelectronics of two-dimensional transition metal dichalcogenides. *Nat. Nanotechnol.* **2012**, *7*, 699−712.
(3) Lembke, D.; Bertolazzi, S.; Kis, A. Single-layer MoS_2 electronics. *Acc. Chem. Res.* **2015**, *48*, 100−110.
(4) Perkins, F. K.; Friedman, A. L.; Cobas, E.; Campbell, P. M.; Jernigan, G. G.; Jonker, B. T. Chemical Vapor Sensing with Monolayer MoS_2. *Nano Lett.* **2013**, *13*, 668−673.
(5) Lee, K.; Gatensby, R.; McEvoy, N.; Hallam, T.; Duesberg, G. S. High-Performance Sensors Based on Molybdenum Disulfide Thin Films. *Adv. Mater.* **2013**, *25*, 6699−6702.
(6) Chhowalla, M.; Shin, H. S.; Eda, G.; Li, L.-J.; Loh, K. P.; Zhang, H. The chemistry of two-dimensional layered transition metal dichalcogenide nanosheets. *Nat. Chem.* **2013**, *5*, 263−275.
(7) Zhang, J.; Yu, H.; Chen, W.; Tian, X.; Liu, D.; Cheng, M.; Xie, G.; Yang, W.; Yang, R.; Bai, X.; Shi, D.; Zhang, G. Scalable Growth of High-Quality Polycrystalline MoS_2 Monolayers on SiO_2 with Tunable Grain Sizes. *ACS Nano* **2014**, *8*, 6024−6030.
(8) Chen, J.; Tang, W.; Tian, B.; Liu, B.; Zhao, X.; Liu, Y.; Ren, T.; Liu, W.; Geng, D.; Jeong, H. Y.; Shin, H. S.; Zhou, W.; Loh, K. P. Chemical Vapor Deposition of High-Quality Large-Sized MoS_2 Crystals on Silicon Dioxide Substrates. *Adv. Sci.* **2016**, *3*, 1500033.
(9) Pyeon, J. J.; Kim, S. H.; Jeong, D. S.; Baek, S.-H.; Kang, C.-Y.; Kim, J.-S.; Kim, S. K. Wafer-scale growth of MoS_2 thin films by atomic layer deposition. *Nanoscale* **2016**, *8*, 10792−10798.
(10) Jin, Z.; Shin, S.; Kwon, D. H.; Han, S.-J.; Min, Y.-S. Novel chemical route for atomic layer deposition of MoS_2 thin film on SiO_2/Si substrate. *Nanoscale* **2014**, *6*, 14453−14458.
(11) Huang, J.-K.; Pu, J.; Hsu, C.-L.; Chiu, M.-H.; Juang, Z.-Y.; Chang, Y.-H.; Chang, W.-H.; Iwasa, Y.; Takenobu, T.; Li, L.-J. Large-Area Synthesis of Highly Crystalline WSe_2 Monolayers and Device Applications. *ACS Nano* **2014**, *8*, 923−930.
(12) Wu, C.-R.; Chang, X.-R.; Chu, T.-W.; Chen, H.-A.; Wu, C.-H.; Lin, S.-Y. Establishment of 2D Crystal Heterostructures by Sulfurization of Sequential Transition Metal Depositions: Preparation, Characterization, and Selective Growth. *Nano Lett.* **2016**, *16*, 7093−7097.
(13) Ettema, A. R. H. F.; de Groot, R. A.; Haas, C.; Turner, T. S. Electronic structure of SnS deduced from photoelectron spectra and band-structure calculations. *Phys. Rev. B: Condens. Matter Mater. Phys.* **1992**, *46*, 7363−7373.
(14) Albers, W.; Haas, C.; Vink, H. J.; Wasscher, J. D. Investigations on SnS. *J. Appl. Phys.* **1961**, *32*, 2220−2225.
(15) Mutlu, Z.; Wu, R. J.; Wickramaratne, D.; Shahrezaei, S.; Liu, C.; Temiz, S.; Patalano, A.; Ozkan, M.; Lake, R. K.; Mkhoyan, K. A.; Ozkan, C. S. Phase Engineering of 2D Tin Sulfides. *Small* **2016**, *12*, 2998−3004.
(16) Yang, Y. B.; Dash, J. K.; Xiang, Y.; Wang, Y.; Shi, J.; Dinolfo, P. H.; Lu, T. M.; Wang, G. C. Tuning the Phase and Optical Properties of Ultrathin SnS_x Films. *J. Phys. Chem. C* **2016**, *120*, 13199−13214.
(17) Ham, G.; Shin, S.; Park, J.; Choi, H.; Kim, J.; Lee, Y.-A.; Seo, H.; Jeon, H. Tuning the Electronic Structure of Tin Sulfides Grown by Atomic Layer Deposition. *ACS Appl. Mater. Interfaces* **2013**, *5*, 8889−8896.
(18) Browning, R.; Plachinda, P.; Padigi, P.; Solanki, R.; Rouvimov, S. Growth of multiple WS2/SnS layered semiconductor heterojunctions. *Nanoscale* **2016**, *8*, 2143−2148.
(19) Dasgupta, N. P.; Meng, X.; Elam, J. W.; Martinson, A. B. F. Atomic Layer Deposition of Metal Sulfide Materials. *Acc. Chem. Res.* **2015**, *48*, 341−348.
(20) Meng, X.; Libera, J. A.; Fister, T. T.; Zhou, H.; Hedlund, J. K.; Fenter, P.; Elam, J. W. Atomic Layer Deposition of Gallium Sulfide Films Using Hexakis(dimethylamido)digallium and Hydrogen Sulfide. *Chem. Mater.* **2014**, *26*, 1029−1039.
(21) Meng, X.; Comstock, D. J.; Fister, T. T.; Elam, J. W. Vapor-Phase Atomic-Controllable Growth of Amorphous Li2S for High-Performance Lithium−Sulfur Batteries. *ACS Nano* **2014**, *8*, 10963−10972.
(22) Riha, S. C.; Koegel, A. A.; Meng, X.; Kim, I. S.; Cao, Y.; Pellin, M. J.; Elam, J. W.; Martinson, A. B. F. Atomic Layer Deposition of MnS: Phase Control and Electrochemical Applications. *ACS Appl. Mater. Interfaces* **2016**, *8*, 2774−2780.
(23) Han, J. H.; Chung, Y. J.; Park, B. K.; Kim, S. K.; Kim, H. S.; Kim, C. G.; Chung, T. M. Growth of p-Type Tin(II) Monoxide Thin Films by Atomic Layer Deposition from Bis(1-dimethylamino-2-methyl-2propoxy)tin and H_2O. *Chem. Mater.* **2014**, *26*, 6088−6091.
(24) Choi, M.-J.; Cho, C. J.; Kim, K.-C.; Pyeon, J. J.; Park, H.-H.; Kim, H.-S.; Han, J. H.; Kim, C. G.; Chung, T.-M.; Park, T. J.; Kwon, B.; Jeong, D. S.; Baek, S.-H.; Kang, C.-Y.; Kim, J.-S.; Kim, S. K. SnO_2 thin films grown by atomic layer deposition using a novel Sn precursor. *Appl. Surf. Sci.* **2014**, *320*, 188−194.
(25) Kim, S. H.; Baek, I.-H.; Kim, D. H.; Pyeon, J. J.; Chung, T.-M.; Baek, S.-H.; Kim, J.-S.; Han, J. H.; Kim, S. K. Fabrication of high-performance p-type thin film transistors using atomic-layer-deposited SnO films. *J. Mater. Chem. C* **2017**, *5*, 3139−3145.
(26) Herron, S. M.; Tanskanen, J. T.; Roelofs, K. E.; Bent, S. F. Highly Textured Tin(II) Sulfide Thin Films Formed from Sheetlike Nanocrystal Inks. *Chem. Mater.* **2014**, *26*, 7106−7113.
(27) Sinsermsuksakul, P.; Heo, J.; Noh, W.; Hock, A. S.; Gordon, R. G. Atomic Layer Deposition of Tin Monosulfide Thin Films. *Adv. Energy Mater.* **2011**, *1*, 1116−1125.
(28) Vidal, J.; Lany, S.; d'Avezac, M.; Zunger, A.; Zakutayev, A.; Francis, J.; Tate, J. Band-structure, optical properties, and defect physics of the photovoltaic semiconductor SnS. *Appl. Phys. Lett.* **2012**, *100*, 032104.
(29) Abutbul, R. E.; Garcia-Angelmo, A. R.; Burshtein, Z.; Nair, M. T. S.; Nair, P. K.; Golan, Y. Crystal structure of a large cubic tin monosulfide polymorph: an unraveled puzzle. *CrystEngComm* **2016**, *18*, 5188−5194.
(30) Abutbul, R. E.; Segev, E.; Zeiri, L.; Ezersky, V.; Makov, G.; Golan, Y. Synthesis and properties of nanocrystalline π-SnS - a new cubic phase of tin sulphide. *RSC Adv.* **2016**, *6*, 5848−5855.
(31) Rabkin, A.; Samuha, S.; Abutbul, R. E.; Ezersky, V.; Meshi, L.; Golan, Y. New Nanocrystalline Materials: A Previously Unknown Simple Cubic Phase in the SnS Binary System. *Nano Lett.* **2015**, *15*, 2174−2179.
(32) Bilousov, O. V.; Ren, Y.; Törndahl, T.; Donzel-Gargand, O.; Ericson, T.; Platzer-Björkman, C.; Edoff, M.; Hägglund, C. Atomic Layer Deposition of Cubic and Orthorhombic Phase Tin Monosulfide. *Chem. Mater.* **2017**, *29*, 2969−2978.
(33) Mathews, N. R.; Anaya, H. B. M.; Cortes-Jacome, M. A.; Angeles-Chavez, C.; Toledo-Antonio, J. A. Tin Sulfide Thin Films by Pulse Electrodeposition: Structural, Morphological, and Optical Properties. *J. Electrochem. Soc.* **2010**, *157*, H337−H341.
(34) Chandrasekhar, H. R.; Humphreys, R. G.; Zwick, U.; Cardona, M. Infrared and Raman spectra of the IV-VI compounds SnS and SnSe. *Phys. Rev. B* **1977**, *15*, 2177−2183.
(35) Ahmet, I. Y.; Hill, M. S.; Johnson, A. L.; Peter, L. M. Polymorph-Selective Deposition of High Purity SnS Thin Films from a Single Source Precursor. *Chem. Mater.* **2015**, *27*, 7680−7688.

DOI: 10.1021/acs.chemmater.7b01856
Chem. Mater. 2017, 29, 8100−8110

(36) Park, H. K.; Jo, J.; Hong, H. K.; Song, G. Y.; Heo, J. Structural, optical, and electrical properties of tin sulfide thin films grown with electron-beam evaporation. *Curr. Appl. Phys.* **2015**, *15*, 964−969.
(37) Zhou, X.; Zhang, Q.; Gan, L.; Li, H.; Zhai, T. Large-Size Growth of Ultrathin SnS_2 Nanosheets and High Performance for Phototransistors. *Adv. Funct. Mater.* **2016**, *26*, 4405−4413.
(38) Lee, Y.-H.; Zhang, X.-Q.; Zhang, W.; Chang, M.-T.; Lin, C.-T.; Chang, K.-D.; Yu, Y.-C.; Wang, J. T.-W.; Chang, C.-S.; Li, L.-J.; Lin, T.-W. Synthesis of Large-Area MoS_2 Atomic Layers with Chemical Vapor Deposition. *Adv. Mater.* **2012**, *24*, 2320−2325.
(39) Kong, D.; Wang, H.; Cha, J. J.; Pasta, M.; Koski, K. J.; Yao, J.; Cui, Y. Synthesis of MoS_2 and $MoSe_2$ Films with Vertically Aligned Layers. *Nano Lett.* **2013**, *13*, 1341−1347.
(40) Zhang, X.; Meng, F.; Christianson, J. R.; Arroyo-Torres, C.; Lukowski, M. A.; Liang, D.; Schmidt, J. R.; Jin, S. Vertical Heterostructures of Layered Metal Chalcogenides by van der Waals Epitaxy. *Nano Lett.* **2014**, *14*, 3047−3054.
(41) Petrov, I.; Barna, P. B.; Hultman, L.; Greene, J. E. Microstructural evolution during film growth. *J. Vac. Sci. Technol., A* **2003**, *21*, S117−S128.
(42) Lee, E. Y. M.; Tran, N. H.; Russell, J. J.; Lamb, R. N. Structure Evolution in Chemical Vapor-Deposited ZnS Films. *J. Phys. Chem. B* **2003**, *107*, 5208−5211.
(43) Bales, G. S.; Redfield, A. C.; Zangwill, A. Growth Dynamics of Chemical Vapor Deposition. *Phys. Rev. Lett.* **1989**, *62*, 776−779.
(44) Kim, J. Y.; George, S. M. Tin Monosulfide Thin Films Grown by Atomic Layer Deposition Using Tin 2,4-Pentanedionate and Hydrogen Sulfide. *J. Phys. Chem. C* **2010**, *114*, 17597−17603.
(45) Ahn, J.-H.; Lee, M.-J.; Heo, H.; Sung, J. H.; Kim, K.; Hwang, H.; Jo, M.-H. Deterministic Two-Dimensional Polymorphism Growth of Hexagonal n-Type SnS_2 and Orthorhombic p-Type SnS Crystals. *Nano Lett.* **2015**, *15*, 3703−3708.
(46) Ran, F.-Y.; Xiao, Z.; Hiramatsu, H.; Ide, K.; Hosono, H.; Kamiya, T. SnS thin films prepared by H_2S-free process and its p-type thin film transistor. *AIP Adv.* **2016**, *6*, 015112.
(47) Sucharitakul, S.; Rajesh Kumar, U.; Sankar, R.; Chou, F.-C.; Chen, Y.-T.; Wang, C.; He, C.; He, R.; Gao, X. P. A. Screening limited switching performance of multilayer 2D semiconductor FETs: the case for SnS. *Nanoscale* **2016**, *8*, 19050−19057.
(48) Caraveo-Frescas, J. A.; Nayak, P. K.; Al-Jawhari, H. A.; Granato, D. B.; Schwingenschlögl, U.; Alshareef, H. N. Record Mobility in Transparent p-Type Tin Monoxide Films and Devices by Phase Engineering. *ACS Nano* **2013**, *7*, 5160−5167.
(49) Wang, Z.; Nayak, P. K.; Caraveo-Frescas, J. A.; Alshareef, H. N. Recent Developments in p-Type Oxide Semiconductor Materials and Devices. *Adv. Mater.* **2016**, *28*, 3831−3892.
(50) Wang, J.; Lian, G.; Xu, Z.; Fu, C.; Lin, Z.; Li, L.; Wang, Q.; Cui, D.; Wong, C.-P. Growth of Large-Size SnS Thin Crystals Driven by Oriented Attachment and Applications to Gas Sensors and Photodetectors. *ACS Appl. Mater. Interfaces* **2016**, *8*, 9545−9551.
(51) Cho, B.; Hahm, M. G.; Choi, M.; Yoon, J.; Kim, A. R.; Lee, Y.-J.; Park, S.-G.; Kwon, J.-D.; Kim, C. S.; Song, M.; Jeong, Y.; Nam, K.-S.; Lee, S.; Yoo, T. J.; Kang, C. G.; Lee, B. H.; Ko, H. C.; Ajayan, P. M.; Kim, D.-H. Charge-transfer-based Gas Sensing Using Atomic-layer MoS_2. *Sci. Rep.* **2015**, *5*, 8052.
(52) Yang, S.; Jiang, C.; Wei, S.-h. Gas sensing in 2D materials. *Appl. Phys. Rev.* **2017**, *4*, 021304.
(53) Friedman, A. L.; Keith Perkins, F.; Cobas, E.; Jernigan, G. G.; Campbell, P. M.; Hanbicki, A. T.; Jonker, B. T. Chemical vapor sensing of two-dimensional MoS2 field effect transistor devices. *Solid-State Electron.* **2014**, *101*, 2−7.
(54) Kim, C. G.; Chung, T. M.; Lee, Y. K.; An, K. S.; Lee, S. S.; Ryu, B. H.; Jang, S. J., Tin amino-alkoxide complexes and process for preparing thereof. U.S. Patent US 8030507 B2, October 4, 2011.

DOI: 10.1021/acs.chemmater.7b01856
Chem. Mater. 2017, 29, 8100−8110